電気学会研究会資料（半導体電力変換 / 家電・民生 / 自動車合同研究会） SPC-23-259
The papers of Joint Technical Meeting on “Semiconductor Power Converter”, HCA-23-049
“Home and Consumer Appliances” and “Vehicle Technology”, IEE Japan VT-23-042

Basic Study on Ground Coil Current Control for WPT with the Consideration of Time-Varying Mutual-Inductance

Binh-Minh Nguyen*, Ryo Matsumoto, Masahiro Mae, Toshiyuki Fujita, Hiroshi Fujimoto

（The University of Tokyo）

Utilizing the circle criterion, this paper formulates the design condition for the ground coil current control in WPT. The condition properly addresses the time-varying parameter of mutual inductance. The effectiveness of the proposed condition has been verified by theoretical analysis, graphical tests, simulation tests, and experimental tests.

Keywords: absolute stability, current control, wireless power transfer, time-varying system.

1. Introduction

To tackle the main problem of short mileage per charge for electric vehicles (EVs), wireless power transfer (WPT) using magnetic resonance coupling has been considered as one of promising technologies [1]. Especially, dynamic wireless power transfer (DWPT) has attracted much interests recently [2]. As shown in Fig. 1, the mutual inductance M changes in accordance with the coil positions. Thus, M is a time-varying parameter in the DWPT system. Consequently, the coil currents might exaggeratedly exceed the rated value at the charging starting moment, and they might fluctuate during the charging period. Such phenomena increase the device and maintenance costs. Therefore, many previous studies have focused on power transmission by dealing with the primary side control [3] – [6]. A method to improve transient response of the start-up current control using the secondary side was presented [7]. A method, which simultaneously incorporates power and current control, was proposed in [8].

Investigating the literature, we have recognized the following two issues. First, from a practical point of view, it is meaningful to investigate a simple but effective controller that tracks the actual current with the reference value. Almost the previous studies utilized the proportional-integral (PI) controller and neglects the discussion on the suitability and effectiveness of such controller. Second, from a theoretical point of view, it is essential to develop a systematic approach to design and analyze current control with respect to the time-varying parameter M. The study [6] only analyzed the worst case by assuming the coupling coefficient equals to zero. In [4], the one cycle control-proportional differential control was merely designed at a given mutual

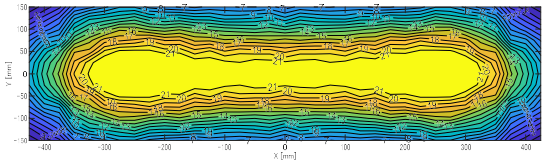

Fig. 1. Example of mutual inductance map of DWPT coils.

inductance. The study [3] experimentally verified that the proposed PI controller is robust to a sharp change of 50% in coupling coefficient. However, this performance was not supported by any theoretical result. Similarly, the study [8] focuses on the problem of maximizing the energy transfer instead of stability analysis.

With respect to the aforementioned issues, this paper focuses on the primary side current control for DWPT with the S-S topology. This paper shows that the system can be modelled as a feedback connection of a time-invariant part and a time-varying part with sector-bounded characteristics. Based on the circle criterion, this paper formulates the design condition that guarantees the absolute stability of the system as the mutual inductance varies between a lower-bound and an upper-bound. The approach allows us a graphical test of system stability, which is convenient for practical application. Utilizing the graphical test, this paper designs a PI controller which allows large position misalignment.

2. Modeling

〈2･1〉 Derivation of the envelop model Fig. 2 shows an S-S equivalent circuit model for the study of WPT. The self-inductance and resonant capacitor of each coil are denoted as L_i and C_i, respectively. The currents are denoted as i_i. The subscripts $i = 1, 2$ mean the primary and secondary sides,

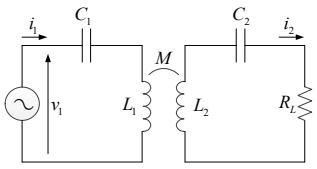

Fig. 2. S-S equivalent circuit model for DWPT.

respectively. The mutual inductance is denoted as M. The load resistance is denoted as R_L. The capacitors are designed to satisfy the following resonance condition:

$$\omega_o^2 L_i C_i = 1 \quad \text{.....(1)}$$

where ω_o is the resonant frequency. The primary voltage is the output of the inverter, and it is originally square waves. Thanks to the bandpass characteristics of the WPT circuit, the currents are sine waves at the resonant frequency. Let $V_1(t)$, $I_1(t)$ and $I_2(t)$ be the fundamental amplitudes of $v_1(t)$, $i_1(t)$, and $i_2(t)$, respectively, the waveforms can be approximately expressed as

$$\begin{cases} v_1(t) = V_1 \sin(\omega_o t) \\ I_{1(2)}(t) = I_{1(2)} \sin(\omega_o t) \end{cases} \quad \text{.....(2)}$$

Appling the Kirchhoff's voltage law to Fig. 2, we have

$$v_1(t) = \frac{1}{C_1}\int i_1(t)dt + (L_1 - M)\frac{di_1(t)}{dt} + M\left(\frac{di_1(t)}{dt} - \frac{di_2(t)}{dt}\right) \quad \text{...(3)}$$

$$M\left(\frac{di_1(t)}{dt} - \frac{di_2(t)}{dt}\right) = (L_2 - M)\frac{di_2(t)}{dt} + \frac{1}{C_2}\int i_2(t)dt + R_L i_2(t) \quad \text{.(4)}$$

Since ω_o is commonly very big, the following approximations can be obtained by neglecting the small terms of high orders [7].

$$\begin{aligned} &\frac{1}{C_1}\int i_1(t)dt = \frac{1}{C_1}\int I_1(t)\sin(\omega_o t)dt \\ &= \frac{-1}{\omega_o C_1}\left(I_1(t)\cos(\omega_o t) - \int \frac{dI_1(t)}{dt}\cos(\omega_o t)dt\right) \quad \text{.....(5)} \\ &\approx \frac{-1}{\omega_o C_1} I_1(t)\cos(\omega_o t) + \frac{1}{\omega_o^2 C_1}\frac{dI_1(t)}{dt}\sin(\omega_o t) \end{aligned}$$

$$\begin{aligned} &M\frac{di_2(t)}{dt} = M\left(\frac{dI_2(t)}{dt}\cos(\omega_o t) - \omega_o I_2(t)\sin(\omega_o t)\right) \quad \text{.....(6)} \\ &\approx -\omega_o M I_2(t)\sin(\omega_o t) \end{aligned}$$

Substituting (2) into (3) and (4) with respect to (1), (5) and (6), the following equations are derived, respectively.

$$V_1(t) = 2L_1\frac{dI_1(t)}{dt} + \omega_o M I_2(t) \quad \text{.....(7)}$$

$$\omega_o M I_1(t) = 2L_2\frac{dI_2(t)}{dt} + R_L I_2(t) \quad \text{.....(8)}$$

From (7) and (8), the envelop model is derived as follows:

$$R_L V_1 + 2L_2\frac{dV_1(t)}{dt} = 4L_1L_2\frac{d^2I_1(t)}{dt^2} + 2L_1R_L\frac{dI_1(t)}{dt} + (\omega_o M)^2 I_1(t) \quad \text{..(9)}$$

Applying the Laplace transformation to (9), the transfer function from V_1 to I_1 can be written as:

$$G(s) = \frac{\frac{1}{2L_1}s + \frac{R_L}{4L_1L_2}}{s^2 + \frac{R_L}{2L_2}s + \frac{(\omega M)^2}{4L_1L_2}} = \frac{\beta_1 s + \beta_0}{s^2 + \alpha_1 s + \alpha_0} \quad \text{.....(10)}$$

〈2·2〉 Block diagram representation This study examined the DWPT system with the parameters summarized in Table 1. M_{min} is the minimum allowable mutual inductance for starting power transmission. Fig. 3 shows the Bode diagram of $G(s)$ with different values of M between M_{min} and M_{max}.

To rigorously treat the time-variation of M, our idea is to equivalently represent $G(s)$ as the feedback connection system in Fig. 4 where:

$$P_1(s) = \frac{\beta_1 s + \beta_0}{s^2 + \alpha_1 s},\ P_2(s) = \frac{\gamma}{s^2 + \alpha_1 s},\ \gamma = \frac{1}{4L_1L_2} \quad \text{.....(11)}$$

$$\varphi(t) = \omega^2 M^2 \quad \text{.....(12)}$$

Table 1. Parameters of DWPT system used in this study.

Parameter	Meaning	Value
L_1	Primary coil inductance	246 μH
L_2	Secondary coil inductance	106 μH
R_L	Load resistance	5.7 Ω
ω	Resonant frequency	$2\pi \times 85000\ rad/s$
M_{min}	Minimum mutual inductance	5 μH
M_{max}	Maximum mutual inductance	20 μH
$V_{1,max}$	Maximum voltage of inverter	30 V
T_d	Delay of sensor measurement	20 μs

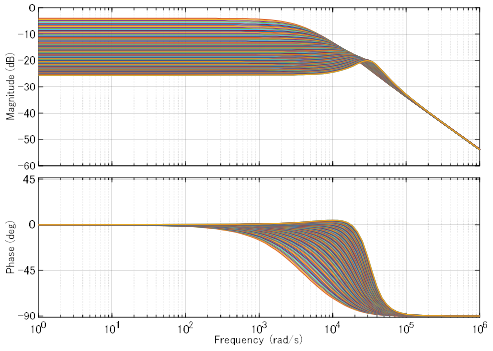

Fig. 3. Bode diagram of $G(s)$ with $M \in [M_{min}, M_{max}]$.

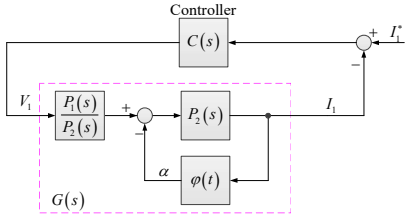

Fig. 4. Block diagram of the primary current control system.

3. Stability condition of current control system

〈3･1〉 Problem setting The study of this paper is based on the current control system shown in Fig. 4. How to detect the starting moment of WPT [7] and how to calculate the reference current I_1^* [8] is not the main goal of this paper. $C(s)$ is the controller to be designed. It outputs the voltage signal V_1 which can be realized by adjusting the width of switching pulses of the primary side inverter. From (12), $\varphi(t)$ varies between a lower-bound $\underline{\varphi} = \omega^2 M_{min}^2$ and an upper-bound $\overline{\varphi} = \omega^2 M_{max}^2$.

〈3･2〉 Stability condition The stability of the system in Fig. 4 can be discussed via the feedback connection of $H(s)$ and $\varphi(t)$ in Fig. 5, where:

$$H(s) = \frac{P_2(s)}{1 + C(s)P_1(s)} \quad \cdots\cdots (13)$$

Applying the circle criterion with Theorem 7.2 in [9], the stability condition can be stated as follows:

Stability condition: The current control system is absolutely stable if the Nyquist plot of $H(j\omega)$ does not enter disk $\mathcal{D}$ defined by $\underline{\varphi}$ and $\overline{\varphi}$ in Fig.6.

4. System analysis with simulation demonstration

〈4･1〉 Conventional PI control design We firstly examine a conventional design approach which neglects the variation of the mutual induction. To this end, we consider the WPT system with the parameters shown in Table 1. The nominal transfer function from V_1 to I_1 is expressed as:

$$G_n(s) = \frac{\beta_1 s + \beta_0}{s^2 + \alpha_1 s + \alpha_{0n}}, \quad \alpha_{0n} = \frac{(\omega M_n)^2}{4 L_1 L_2} \quad \cdots\cdots (14)$$

For instance, M_n is set as the value when there are no misalignments between two coils ($M_n = 19.5\mu H$). By a fine-tuning process using the nominal plant, we select the PI controller $C(s) = K_p + K_i/s$ with $K_p = 0.677$, $K_i = 2.041 \times 10^5$. With this selection, the nominal close-loop transfer function $P_{cln}(s) = C(s)G_n(s)/[1 + C(s)G_n(s)]$ has stable poles $-20.16 \pm 548.70j$ and -3.70×10^7. However, $H(j\omega)$ enters the disk $\mathcal{D}$,

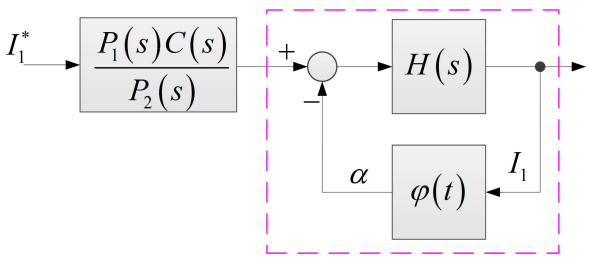

Fig. 5. Equivalent diagram of the current control system.

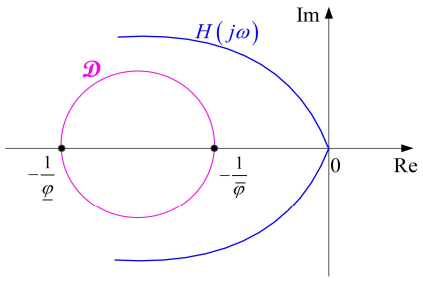

Fig. 6. Definition of disk $\mathcal{D}$.

as shown in Fig. 7. This means the actual system does not satisfy the absolute stability condition. To validate this conclusion, simulation tests were conducted as follows with the reference current of 1.5 A.

Case A: The positions of two coils are fixed, such that there is no misalignment between them. In this case, the mutual inductance always equals to the nominal value (see Fig. 8a). A good current tracking performance can be realized as shown in Fig. 8b.

Case B: The power transmission starts with a large misalignment between two coils, such that the mutual inductance varies from the minimum value (see Fig. 8a). Consequently, the current vibrates seriously (see Fig. 8b).

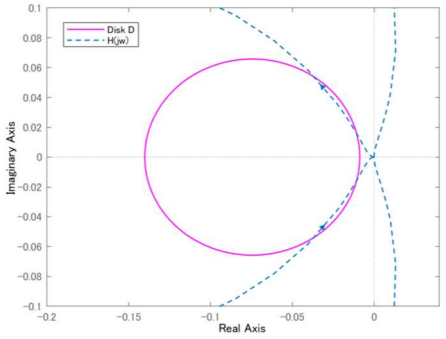

Fig. 7. Graphical test: conventional PI controller design.

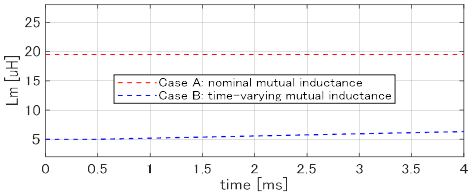

(a) Mutual inductance.

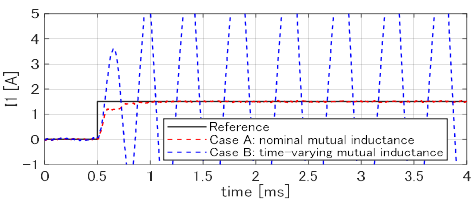

(b) Envelope current.

Fig. 8. Simulation test: conventional PI controller design.

〈4･2〉 Proposed PI control design Substitute (11) into (13) with the notice that $\beta_0 = \beta_1\alpha_1$, $H(s)$ is written as follows with the PI controller

$$H(s) = \frac{\gamma s}{(s+\alpha_1)\left(s^2 + \beta_1 K_p s + \beta_1 K_i\right)} \quad \text{.....(15)}$$

It can be seen that the poles of $H(s)$ are also the poles of $P_{cl}(s)$ from I_1^* to I_1 in the worst case such that the mutual inductance is zero. The real and imaginary parts of $H(j\omega)$ are:

$$\mathrm{Re}_H = \frac{\gamma\omega^2\left(\beta_1 K_i + \alpha_1\beta_1 - \omega^2\right)}{\left(\omega^2+\alpha_1^2\right)\left[\left(\beta_1 K_i - \omega^2\right)^2 + \beta_1^2 K_p^2\omega^2\right]} \quad \text{.....(16)}$$

$$\mathrm{Im}_H = \frac{\gamma\omega\left[\alpha_1\beta_1 K_i - \left(\alpha_1 + \beta_1 K_p\right)\omega^2\right]}{\left(\omega^2+\alpha_1^2\right)\left[\left(\beta_1 K_i - \omega^2\right)^2 + \beta_1^2 K_p^2\omega^2\right]} \quad \text{.....(17)}$$

Solving $\mathrm{Re}_H = 0$, it can be found that $H(j\omega)$ intersects with the imaginary axis at two points symmetrical about the real axis.

Solving $\mathrm{Im}_H = 0$, $H(j\omega)$ is shown to intersect with the real axis at two separate points. One point is the origin, and the other point is placed at the right-hand side of the imaginary axis. The distance L between two points is $Re_H(\omega_{im})$, where:

$$\omega_{im} = \sqrt{\frac{\alpha_1\beta_1 K_i}{\alpha_1 + \beta_1 K_p}} \quad \text{.....(18)}$$

is the non-zero solution of the equation $\mathrm{Im}_H = 0$.

From (15), $H(s)$ has a stable pole which equals to $-\alpha_1$. Placing other two poles at the stable value $-\rho$, we have

$$s^2 + \beta_1 K_p s + \beta_1 K_i \equiv (s+\rho)^2 \Leftrightarrow \begin{cases} K_p = 2\beta_1^{-1}\rho \\ K_i = \beta_1^{-1}\rho^2 \end{cases} \quad \text{.....(19)}$$

The maximum value of the inverter voltage should be considered when designing the feedback controller. Thus, ρ should be limited by a threshold $\overline{\rho}$. If ρ is chosen bigger than this threshold, the system might suffer fluctuation due to the saturation of the inverter voltage. Recently, we proposed in IEEE-IECON 2023 a method to rigorously design the feedback controller with respect to the saturation of the control signal [10]. This paper aims at a practical design for current control in DWPT. Therefore, we considered the following strategy for tuning ρ. The selected ρ must satisfy the graphical test given by the stability condition, and a simulation test by performing a simulator that imitates the real DWPT system shown in Table 1. In this study, Matlab/Simulink R2021b is used to establish the simulator. The simulation test is the same as Case B presented in the previous sub-section.

Step 1 (Rough tuning): By increasing ρ, we find the upper-bound $\overline{\rho}$ such that the current start to fluctuate.

Step 2 (Fine tuning): The range from 0 to $\overline{\rho}$ divided by N steps.

For $k = 1:N$

- Calculate the PI gains using (19) with $\rho = (\overline{\rho}/N)k$.
- *Graphical test*: Verify if the Nyquist plot of $H(j\omega)$ does not enter disk $\mathcal{D}$ or not.
- *Simulation test*: Verify if the controller satisfies the required performance of settling time and overshoot, and the saturation of the inverter voltage does not occur.

The upper-bound is found to be $\overline{\rho} = 3.6 \times 10^4$. The fine-tuning was performed with $N = 100$. This paper demonstrates the results of some steps $k = \{2, 10, 28, 56, 100\}$ for clear discussion. The graphical test and simulation test are summarized in Figs. 9 and 10, respectively. At all steps, the Nyquist plot of $H(j\omega)$ does not enter disk $\mathcal{D}$. Furthermore, it can be shown that:

- If ρ is too small (i.e., $k = 2$), the tracking performance is very poor. By increasing ρ (i.e., $k = 10$), the tracking performance can be improved.
- If ρ is too big (i.e., $k = 56$), the steady state error and the settling time can be further enhanced. However, the overshoot is increased. For the safety of the DWPT system, this overshoot is not allowable.
- If ρ reaches the upper-bound at $k = 100$, the fluctuation happens due to the voltage saturation.

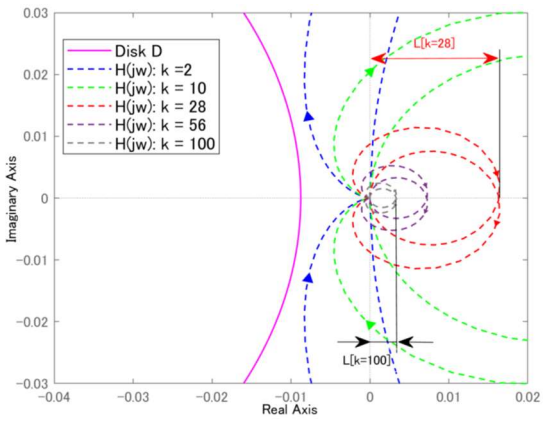

Fig. 9. Graphical test: proposed PI controller design.

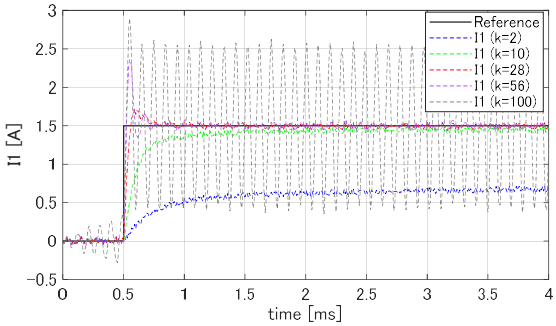

Fig. 10. Simulation test: proposed PI controller design.

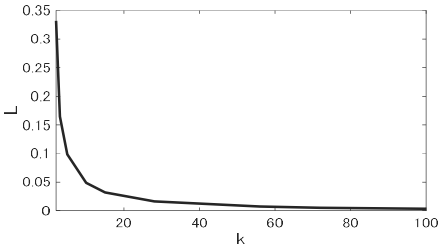

Fig. 11. Relationship between L and desired poles.

To compromise the aforementioned trade-off, it is possible to select the desired pole at $k = 28$ ($\rho = 3.6 \times 10^4$). With this selection, the system only suffers a small overshoot of 13% even if the power transmission starts at M_{min}.

The relationship between the distance L and the desired poles are shown in Fig. 11. The increasing of ρ results in the decreasing of L. When $\rho = \overline{\rho}$ or $k = N = 100$, the distance L is reduced to the minimum value of 0.0033. With the selected poles at $k = 28$, the distance is 0.0164. With $k = 2$, the distance is increased to 0.2475. From this discussion, the distance L can be used as an index to select the desired poles to compromise the trade-off between steady state error and transient overshoot.

Varying the coil inductances and the load resistance in the range of $[+20\%, -20\%]$ around the nominal values, the Nyquist plots of $H(j\omega)$ with $k = 28$ are shown in Fig. 12. It can be recognized that, the proposed PI controller guarantees a certain level of robustness under model uncertainty.

5. Experimental validation

〈5·1〉 Experimental setting Fig. 13 describes the test-bench with the nominal parameters shown in Table 1. This testbench allows us to adjust the relative position between the primary coil and secondary coil. A FPGA board is used to calculate the envelop of the current. The PE-Expert4 computer serves as the main controller. C programing is used to perform the feedback current control, display and store the experimental data. The

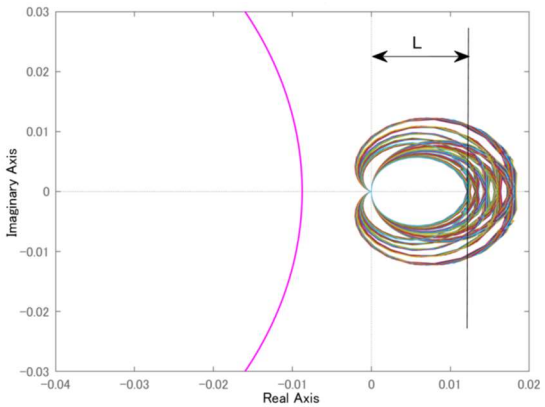

Fig. 12. Robustness of the proposed PI controller with $k = 28$.

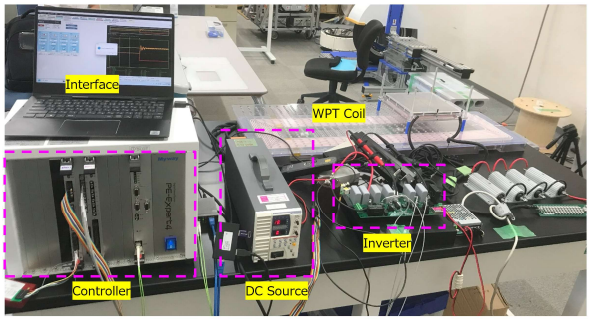

Fig. 13. Testbench system.

control period of the system is $5.9\ \mu s$.

〈5·2〉 Experimental results Several tests we performed, and there results are summarized in Fig. 14.

Test 1 (*Without current control*): The longitudinal and lateral misalignments are set to be zero. The duty cycle of the inverter is fixed at 0.5. As can be seen in Fig. 14a, the current reaches a peak value which is more than 2 times of the reference value. The current overshoot would be more serious if the coil misalignments are non-zero.

Test 2 (*PI controller designed by conventional approach*): This test is to evaluate the PI controller obtained in sub-section 4.1. The power transmission starts at the longitudinal and lateral misalignments of 450 mm and 60 mm, respectively. Hence, the mutual inductance is only $5.5\ \mu H$. As shown in Fig. 14b, the current fluctuates considerably as the power transmission starts. This result, which is a failure example of the conventional approach, matches with the theoretical analysis in previous section.

Test 3 (*PI controller designed by proposed approach*): The power transmission starts with large longitudinal and lateral misalignments, which are similar to that of Test 2. As can be seen in Fig. 14c, the envelop current quickly follows the reference value. The overshoot is reduced to approximately 75% in comparison with that of **Test 1**.

6. Conclusions

Using the Circle criterion, this paper formulates the stability condition for the ground coil current control in DWPT. The condition properly addresses the time-varying parameter of mutual inductance. Thanks to the graphical test, the condition allows us a practical approach to analyze and tune the current controller. Testbench experiments show that stable current control can be achieved with less overshoot, even if the system suffers a large misalignment between two coils.

However, this paper only performed power transfer in a short period of time. Also, the compensation of current delay was not considered in this paper. In future, we will develop the controller

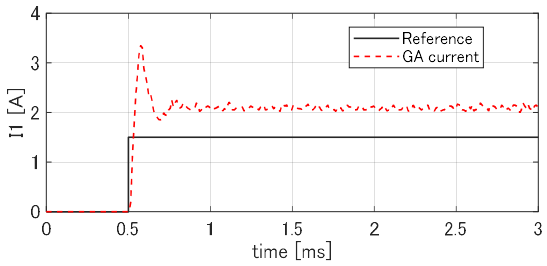

(a) Test 1: without current control.

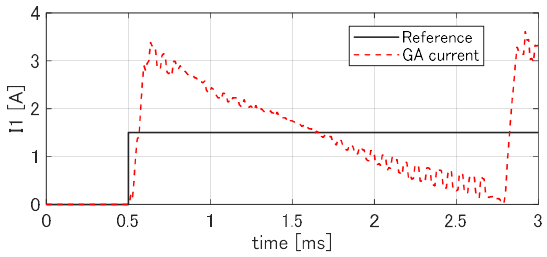

(b) Test 2: PI controller designed by conventional approach.

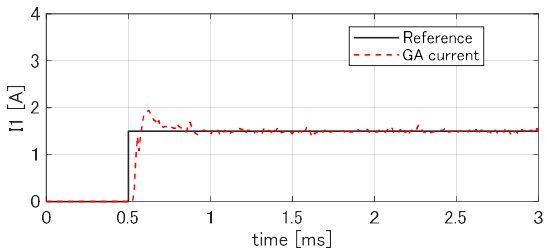

(c) Test 3: PI controller designed by proposed approach.

Fig. 14. Experimental results of envelope current.

to compensate the delay of sensor measurement. Experiments with higher power using moving coil will be conducted to further evaluate the proposal of this paper. Besides, we are interested in the power control in the outer loop to properly generate the reference current. Furthermore, the proposed method will be extended to current control in both primary and secondary sides.

Acknowledgements

This research is based on results obtained from a project, JPNP21005, subsidized by the New Energy and Industrial Technology Development Organization (NEDO).

References

(1) T. Newbolt, P. Mandal, H. Wang, and R. Zane, "Sustainability of Dynamic Wireless Power Transfer Roadway for In-motion Electric Vehicle Charging," IEEE Transactions on Transportation Electrification, 2023 (Early Access).

(2) K. Tomoaki, B.-M. Nguyen, S. Osamu, Y. Shota, and H. Fujimoto, "Lateral Misalignment and Yaw Angle Control Considering Vehicle Dynamics Based on Receiving Energy in Dynamic Wireless Power Transfer," IFAC World Congress, 2023.

(3) J. Jiang, K. Song, Z. Li, C. Zhu, and Q. Zhang, "System Modeling and Switching Control Strategy of Wireless Power Transfer System," IEEE Journal of Emerging and Selected Topics in Power Electronics, Vol. 6, No. 3, pp. 1295-1305, 2018.

(4) W. Shi, J. Deng, Z. Wang, and X. Cheng, "The Start-up Dynamic Analysis and One Cycle Control-PD Control Combined Strategy for Primary-Side Controlled Wireless Power Transfer System," IEEE Access, Vol. 6, pp. 14439-14450, 2018.

(5) J. Noeren and N. Parspour, "Model Predictive Control for Contactless Energy Transfer Systems," IEEE PELS Workshop on Emerging Technologies: Wireless Power Transfer, pp. 6-9, 2020.

(6) K. Hata, T. Imura, H. Fujimoto, and Y. Hori, "Soft-Start Control Method for In-motion Charging of Electric Vehicles Based on Transient Analysis of Wireless Power Transfer System," IEEE Energy Conversion Congress and Exposition, pp. 2009-2015, 2018.

(7) T. Hamada, T. Fujita, and H. Fujimoto, "Fast Start-Up Control of Both-Side Current without Overshoot Focusing on Rectification Timing for Dynamic Wireless Power Transfer Systems," IEEE Journal of Emerging and Selected Topics in Industrial Electronics, 2023 (Early Access).

(8) G. Guidi, J. A. Suul, and H. Fujimoto, "Conditions for Maximum Energy Transfer in Inductive Road-Powered Electric Vehicle Applications Taking System Limitation into Account," 5th International Electric Vehicle Technology Conference, 2021.

(9) H. Khalil, "Nonlinear Systems," Prentice Hall (2002).

(10) T. Ueno, B-M. Nguyen, and H. Fujimoto, "Driving Force Control for In-Wheel Motor Electric Vehicles with Wheel Speed Limiter and Absolute Stability Analysis," 49th Annual Conference of the IEEE Industrial Electronics Society, 2023 (Accepted).